LAWRENCE
LIVERMORE
NATIONAL
LABORATORY

UCRL-BOOK-212729

Development and Application of Compatible Discretizations of Maxwell's Equations

D. White, J. Koning, R. Rieben

June 6, 2005

This work was performed under the auspices of the U.S. Department of Energy by University of California, Lawrence Livermore National Laboratory under Contract W-7405-Eng-48.

DEVELOPMENT AND APPLICATION OF COMPATIBLE DISCRETIZATIONS OF MAXWELL'S EQUATIONS *

D. WHITE †, J. KONING ‡, AND R. RIEBEN §

Abstract.
We present the development and application of compatible finite element discretizations of electromagnetics problems derived from the time dependent, full wave Maxwell equations. We review the $H(curl)$-conforming finite element method, using the concepts and notations of differential forms as a theoretical framework. We chose this approach because it can handle complex geometries, it is free of spurious modes, it is numerically stable without the need for filtering or artificial diffusion, it correctly models the discontinuity of fields across material boundaries, and it can be very high order. Higher-order $H(curl)$ and $H(div)$ conforming basis functions are not unique and we have designed an extensible C++ framework that supports a variety of specific instantiations of these such as standard interpolatory bases, spectral bases, hierarchical bases, and semi-orthogonal bases. Virtually any electromagnetics problem that can be cast in the language of differential forms can be solved using our framework. For time dependent problems a method-of-lines scheme is used where the Galerkin method reduces the PDE to a semi-discrete system of ODE's, which are then integrated in time using finite difference methods. For time integration of wave equations we employ the unconditionally stable implicit Newmark-Beta method, as well as the high order energy conserving explicit Maxwell Symplectic method; for diffusion equations, we employ a generalized Crank-Nicholson method. We conclude with computational examples from resonant cavity problems, time-dependent wave propagation problems, and transient eddy current problems, all obtained using the authors massively parallel computational electromagnetics code *EMSolve* .

Key words.
Computational electromagnetics, Maxwell's equations, vector finite elements, high order methods, $H(curl)$ and $H(div)$ - conforming methods, discrete differential forms, spurious modes, numerical dispersion, wave propagation, transient eddy currents, electromagnetic diffusion

1. Introduction. The equations of electromagnetics can be simply and elegantly cast in the language of differential geometry, more precisely in terms of differential forms or p-forms [1], [2], [3]. In this geometrical setting, the fundamental conservation laws are not obscured by the details of coordinate system dependent notation; and, the governing equations can be reformulated in a more compact and clear way using well known differential operators of the exterior algebra such as the exterior derivative, the wedge product, and the Hodge star operator, see [4] for an introduction to differential forms. In this context, a natural framework for the modeling of electromagnetics is provided. For example, the electric potentials can be represented by 0-forms; electric and magnetic fields by 1-forms; electric and magnetic fluxes by 2-forms; and scalar charge density by 3-forms.

*This work was performed under the auspices of the U.S. Department of Energy by the University of California, Lawrence Livermore National Laboratory under contract No. W-7405-Eng-48

†Defense Sciences Engineering Division, Lawrence Livermore National Laboratory, white37@llnl.gov

‡Defense Sciences Engineering Division, Lawrence Livermore National Laboratory, koning1@llnl.gov

§Defense Sciences Engineering Division, Lawrence Livermore National Laboratory, rieben1@llnl.gov

In the context of Galerkin approximations, the choice of the finite element space plays a crucial role in the stability and convergence of the discretization. For instance, in numerical approximations of the magnetic and electric field intensities, $H(curl)$ -conforming finite element spaces (or edge elements) are preferred over traditional nodal vector spaces since they eliminate spurious modes in eigenvalue computations and they prevent fictitious charge build-up in time-dependent computations. The lowest order $H(curl)$ -conforming basis functions were developed by Whitney [5] before the advent of finite element programs. Arbitrary order versions were introduced by Nédélec [6],[7] as a generalization of the mixed finite element spaces introduced by P.A. Raviart and J.M. Thomas in [8] for $H(div)$ -conforming methods. For an extensive analysis of several $H(div)$ -conforming methods see [9].

Recently, Hiptmair, motivated by the theory of exterior algebra of differential forms, presented a unified framework for the construction of conforming finite element spaces. Remarkably, both $H(curl)$ and $H(div)$ conforming finite element spaces and the definition of their degrees of freedom and interpolation operators can be derived within this framework, see [10] for more details. In simple terms the finite element basis functions satisfy discrete counterparts of the De Rham exact sequence and related commuting diagrams. The architecture of our *EMSolve* software closely mimics the structure of differential forms. In our software terminology, a discrete differential *p*-form is a finite element basis used to discretize a *p*-form field. In *EMSolve* the global discrete exterior derivative and Hodge operators are sparse matrices, and the rules of differential forms define how these matrices can be combined to represent discretizations of PDE's. Given a physical law expressed in the language of differential forms, it is therefore quite straightforward to discretize the problem using *EMSolve* .

One unique feature of *EMSolve* is the emphasis on high-order discretization which can reduce the mesh size, memory usage, and CPU time required to achieve a prescribed error tolerance. This is particularly true for electrically large problems. For these problems it is known that the Galerkin discretization error is larger than the best approximation error of the finite element space. This is sometimes referred to as the pollution effect, and has been more precisely explained in [11],[12]. In the engineering community this is referred to as numerical dispersion, as the computed phase velocity differs from the physical phase velocity and phase error builds up linearly with respect to distance and time. For the popular lowest order edge elements, it is known that the numerical dispersion relation is second order accurate [13], [14],[15]. Second order accuracy may seem adequate, but for an electrically large problem the phase error may be such that the global error is 100 percent even though the local truncation error is quite small. A detailed analysis of dispersion for higher-order $H(curl)$ finite elements on orthogonal Cartesian meshes is given in [16], with the result that the dispersion error is asymptotically $O(h^{2k})$ where k is the order of the basis functions.

It should be noted that there are numerous numerical schemes for electromagnetics that are based in part on differential forms and related geometrical concepts, such as the cell method [17], finite integration theory [18], [19], and

mimetic discretizations [20]. Even the most popular method for time-domain computational electromagnetics, Yee's FDTD method [21], has been reinterpreted from a geometric perspective by numerous authors [22], [23].

2. Numerical Formulation. We begin with the generic boundary value problem stated in the language of differential forms from [24]. This problem statement is generic in that the degree of the forms are not specified. By specifying the degree p we have equations involving the divergence, gradient, or curl operators. We assume a 3-dimensional domain Ω with piecewise smooth boundary $\partial\Omega$ partitioned into Γ_D, Γ_N, and Γ_M. The problem statement is

$$du = (-1)^p \sigma \qquad dj = -\Psi + \Phi \ \textit{in}\ \Omega \tag{2.1}$$

$$T_D u = f \ \textit{on}\ \Gamma_D \qquad T_N j = g \ \textit{on}\ \Gamma_N \tag{2.2}$$

$$j = \star_\alpha \sigma \qquad \Psi = \star_\gamma u \ \textit{in}\ \Omega \tag{2.3}$$

$$T_M j = (-1)^p \star_\beta T_M u \ \textit{on}\ \Gamma_M. \tag{2.4}$$

Here u is a $(p-1)$-form, σ is a p-form, j is a $(3-p)$-form, and both Ψ and Φ are $(3-p+1)$-forms, where $1 \leq p \leq 3$. The variable Φ is a source term. The symbols α, β and γ denote generic material constitutive relations (e.g. electric permittivity or conductivity). In (2.1) the operator d is the exterior derivative which maps p-forms to $(p+1)$-forms. In the boundary conditions (2.2) and (2.4) the symbol T denotes the trace operator, where the trace of a p-form is an integral over a $p-1$-dimensional manifold. In (2.3) and (2.4) the $\star$ symbol denotes the Hodge-star operator, which converts p-forms to $(3-p)$-forms and typically involves material constitutive properties. Equations (2.1) and (2.3) can be combined to yield the general second-order elliptic equation

$$(-1)^p d \star_\alpha du = - \star_\gamma u + \Phi. \tag{2.5}$$

The wedge product of differential forms is used in the definition of bilinear forms. The wedge product of a p-form ω and a q-form η is a $(p+q)$-form ζ

$$\omega^p \wedge \eta^q = \zeta^{(p+q)}, p+q \leq 3.$$

If $p+q=3$ then $\omega^p \wedge \eta^q$ is an volumetric energy density like quantity and can be integrated over a volume to yield energy. If $p+q=2$ then $\omega^p \wedge \eta^q$ is a flux density like quantity and can be integrated over a surface to yield net flux.

A Galerkin finite element solution of the generic second-order equation (2.5) will require bilinear forms. Using the exterior algebra, the bilinear forms required in the Galerkin finite element method can be easily formulated from the general second-order equation (2.5) by taking the wedge product with a $(p-1)$-form v and integrating over the volume Ω,

$$\int_\Omega (-1)^p d \star_\alpha du \wedge v = - \int_\Omega \star_\gamma u \wedge v + \int_\Omega \Phi \wedge v.$$

Using the integration-by-parts formula

$$\int_\Omega d\omega \wedge \eta + (-1)^p \int_\Omega \omega \wedge d\eta = \int_{\partial\Omega} \omega \wedge \eta$$

yields the two key symmetric bilinear forms

$$a(u,v) = \int_\Omega \star_\alpha (du) \wedge dv, \tag{2.6}$$

$$b(u,v) = \int_\Omega \star_\gamma u \wedge v. \tag{2.7}$$

and the additional bilinear forms for source terms and boundary conditions

$$c(u,\Phi) = \int_\Omega u \wedge \Phi$$

$$d(u,g) = \int_{\partial\Omega} \star_\alpha du \wedge g.$$

Let $\mathcal{H}^p = \left\{u \in L_2(\Omega) : |||u|||_p^2 < \infty\right\}$ and $\mathcal{H}_0^p = \left\{u \in \mathcal{H}^p : T_D(u) = 0\right\}$ be generic Hilbert spaces, where $|||u|||_p^2 = \int_\Omega u \wedge \star u + \int_\Omega du \wedge \star du$. Then the Galerkin form of the generic second-order equation (2.5) can now be expressed as follows:

Given the source function Φ and the boundary condition g, find $u \in \mathcal{H}^p$ such that

$$T_D(u) = g \text{ and } a(u,v) = b(u,v) + c(u,\Phi) + d(u,g), \quad \forall v \in \mathcal{H}_0^p.$$

It is not necessary to combine the two 1st-order equations into a single 2nd order equation. If it is desired to formulate the problem as a coupled pair of 1st order equations, as in a mixed method [8], [25], [26], [9], then an additional bilinear form is required, namely

$$e(u,v) = \int_\Omega \star_\alpha (du) \wedge v, \tag{2.8}$$

with the requirement that u is a p-form and v is a $(p+1)$ form. With the generic bilinear forms (2.6), (2.7), and (2.8), source terms, and boundary conditions we can construct a wide variety of model equations that can be solved via the finite element method.

We are primarily concerned with time dependent phenomena. The time derivative does not effect the degree of a form. For the generic wave equation we simply add time derivatives to (2.1) which yields

$$du = (-1)^p \frac{\partial \sigma}{\partial t}, \;\; dj = -\frac{\partial \psi}{\partial t} + \Phi \;\; in \;\; \Omega \tag{2.9}$$

In the Tonti diagram below we show the time-dependent Maxwell's equations, where d denotes the spatial derivative, $\frac{\partial}{\partial t}$ denotes the time derivative and converging arrows denote summation. In these diagrams ϕ is the 0-form scalar potential; the 1-forms A, E, and H are the magnetic vector potential, the electric field, and the magnetic field, respectively; the 2-forms B, D, and J are the magnetic flux density, the electric flux density, and the electric current density, respectively; and ρ is the 3-form scalar charge density. The left diagram encompasses Faraday's

law $dE - \frac{\partial}{\partial t}B = 0$, Coulomb's law for the magnetic field $dB = 0$, and the fact that the electric field E can be written in terms of potentials as $E = d\phi - \frac{\partial}{\partial t}A$. The right diagram encompasses Ampere's law $dH - \frac{\partial}{\partial t}D = J$, Coulomb's law for the electric field $dD = \rho$, and the continuity equation $dJ - \frac{\partial}{\partial t}\rho = 0$. The two diagrams are connected by the constitutive relations $D = \star_\varepsilon E$ and $B = \star_\mu H$.

$$
\begin{array}{lccccc}
0\text{-forms}: & & \phi & & & \\
& & \downarrow d & & & \\
1\text{-forms}: & A & \xrightarrow{-\frac{\partial}{\partial t}} & E & & H \\
& \downarrow d & & \downarrow d & & \downarrow d \\
2\text{-forms}: & B & \xrightarrow{-\frac{\partial}{\partial t}} & 0 & D \xrightarrow{-\frac{\partial}{\partial t}} & J \\
& \downarrow d & & & \downarrow d & \downarrow d \\
3\text{-forms}: & 0 & & & \rho \xrightarrow{-\frac{\partial}{\partial t}} & 0
\end{array}
$$

A wave equation can be derived by combining the two diagrams and solving for E,

$$\frac{\partial^2}{\partial t^2}(\star_\varepsilon E) = d \star_{\mu^{-1}} dE - \frac{\partial}{\partial t} J. \tag{2.10}$$

This wave equation resembles the generic second order equation (2.5) with the addition of temporal derivatives. Clearly, if it is determined that one of the time derivatives is small and can be neglected, the result is an electromagnetic diffusion equation (parabolic PDE). Therefore the same bilinear forms (2.6)) and (2.7) are required for spatial discretization of either the elliptic, hyperbolic (wave equation) or parabolic (diffusion equation) problem.

2.1. Local Finite Element Operations. We follow the work of Ciarlet [27] and adhere to the definition of a finite element as a set of three distinct objects $(\Sigma, \mathcal{P}, \mathcal{A})$ such that:

- Σ is the polyhedral domain over which the element is defined
- $\mathcal{P}$ is a finite dimensional polynomial space from which basis functions are constructed
- $\mathcal{A}$ is a set of linear functionals (*Degrees of Freedom*) dual to $\mathcal{P}$

Let Σ_h be a discretization of the problem domain Ω using tetrahedral, hexahedral, or prismatic elements. By using a local change of variables given by the iso-

parametric mapping $\Phi(\hat{\Sigma}) = \Sigma$, we re-write the bilinear of (2.6) as follows

$$\begin{aligned} a(u,v) &= \int_{\Omega} \star_{\alpha} \, du \wedge dv \\ &= \sum_{\Sigma \in \Sigma_h} \int_{\Sigma = \Phi(\hat{\Sigma})} \star_{\alpha} \, du \wedge dv \\ &= \sum_{\Sigma \in \Sigma_h} \int_{\hat{\Sigma}} (\star_{\alpha} \circ \Phi) \, \Phi^{*} \left(du \wedge dv \right) \, |D\Phi| \\ &= \sum_{\Sigma \in \Sigma_h} \int_{\hat{\Sigma}} (\star_{\alpha} \circ \Phi) \, \Phi^{*}(du) \wedge \Phi^{*}(dv) \, |D\Phi|. \end{aligned} \tag{2.11}$$

Similarly, the bilinear form of (2.7) can be rewritten as

$$b(u,v) = \sum_{\Sigma \in \Sigma_h} \int_{\hat{\Sigma}} (\star_{\beta} \circ \Phi) \, \Phi^{*}(u) \wedge \Phi^{*}(v) \, |D\Phi|. \tag{2.12}$$

Equations (2.11) and (2.12) show that all calculations for the various bilinear forms can be performed on a standard reference element $\hat{\Sigma}$ (i.e. the unit cube, tetrahedron, or prism). Results are then transformed to physical mesh elements (of arbitrary curvature) via a set of well defined transformation rules based on the properties of differential forms. These rules are summarized in Table 1. Given these transformations the bases need only be evaluated on the reference element and transformed accordingly. In *EMSolve* the bilinear form requires that the reference element, the quadrature rule, and the *p*-form basis functions be specified just once. The basis functions are then sampled at the quadrature points on the reference element, and this information is cached for latter use. This gives rise to a very computationally efficient algorithm for computing finite element approximations. For a given element topology and basis order, the basis functions only need to be computed once. Then, for every element of the same topology in the mesh, the results from the reference element can simply be mapped according to the transformation rules. This can significantly reduce computational time for a typical finite element computation. In addition, integration over the reference element is much simpler and can often be done exactly using Gaussian quadrature of the appropriate order.

When implementing a finite element space $\mathcal{P}$ in the context of differential forms, the explicit formulation of the space depends on the *p*-form and the topology of the reference element. The construction of the finite element space $\mathcal{P}$ is not unique, we choose a construction that leads to a simple and efficient implementation. We use uniformly spaced interpolatory polynomials similar to those described in [28] and [29] as a *primitive basis* on a reference element. The actual bases used in the finite element procedure are constructed on this reference element $\hat{\Sigma}$ rather than in the physical coordinate system and are written as a linear combination of the primitive basis. For example, non-uniform interpolatory functions, moment-based functions, orthogonal functions, etc. can all be expressed as a linear combination of the primitive basis

The construction of a p-form basis of order k is as follows. We begin by generating a primitive basis $W = \{w_j\}$. We can then construct a new basis (non-uniform interpolation, hierarchical, etc.) in terms of the primitive bases by imposing a set of constraints of the form

$$\alpha_i(w_j) = \delta_{ij}, \tag{2.13}$$

where $\alpha_i \in \mathcal{A}$ are the known degrees of freedom of the new basis. The degrees of freedom are in general integral moments, but this is not necessary. What is necessary is that the degrees of freedom satisfy the following:

- *Unisolvence*: $\{\alpha_i\}$ is dual to the finite element space $\mathcal{P}$; i.e. there exists a set $\{w_j\} \subset \mathcal{P}$ such that $\alpha_i(w_j) = \delta_{i,j}$.
- *Invariance*: degrees of freedom remain unisolvent upon a change of variables; this implies they are not affected by the pullback operation; i.e. $\Phi^*(\alpha_i) = \hat{\alpha}_i$.
- *Locality*: the trace of a basis function on a sub-simplex is determined by degrees of freedom associated *only* with that sub-simplex.

The procedure requires the formation of a linear system

$$V_{ij} = \alpha_i(w_j); \;\; w_j \in W$$

This system, which is similar to a Vandermonde matrix, is a linear mapping which expresses the new basis in terms of the primitive basis and will have a rank equal to the dimension of the primitive basis. The newly defined basis, which we will denote as W' is given by:

$$W' = V^{-1}W$$

In *EMSolve* , the construction and solution of the Vandermonde system is done once and only once on the reference element. For the evaluation of the basis functions on an actual (or global) element, they are first evaluated on the reference element then transformed according to the transformation rules of Table 1, where the "hat" symbol denotes objects defined with respect to the reference element coordinate system. It is important to note that this process implies that the basis functions have units as shown in Table 2. In standard nodal-based finite element methods the basis functions are dimensionless and the unknowns (the unknown coefficients of the basis function expansion of the field) are simply the value of a field at a point, but here the unknowns are integrals of the field. This seems to be a common theme of all compatible discretization schemes of Maxwell's equations whether they are based upon the finite element method given here, or mimetic finite volume [20] and finite difference [22] methods.

We have a class hierarchy for each of the p-form bases, the partial hierarchy is shown in Figure 1. Concrete classes are presented in the lowest level of the tree. The other p-forms have a similar inheritance diagram. The complete class library is documented in [30], [31], [32]. Our Silvester-Lagrange (SL) bases are similar to the bases defined in [28] which use equidistant and shifted equidistant interpolation points. The difference between our SL bases and the bases proposed in [28]

TABLE 1
Transformation rules Φ^*

	$\Phi^*(u)$	$\Phi^*(du)$
0-forms	$\hat{u}$	$D\Phi^{-1}(d\hat{u})$
1-forms	$D\Phi^{-1}\hat{u}$	$\frac{1}{\lvert D\Phi\rvert}D\Phi^T(d\hat{u})$
2-forms	$\frac{1}{\lvert D\Phi\rvert}D\Phi^T\hat{u}$	$\frac{1}{\lvert D\Phi\rvert}(d\hat{u})$

TABLE 2
Units of Electromagnetic Quantities, Basis Functions, and Degrees-of-Freedom

Form	Basis Function	Electromagnetic Quantity		DOF
0-forms	1	ϕ	$(Volts)$	$Volts$
1-forms	m^{-1}	E	$(Volts/m)$	$Volts$
1-forms	m^{-1}	H	$(Amps/m)$	$Amps$
2-forms	m^{-2}	D	$(Coulombs/m^2)$	$Coulombs$
2-forms	m^{-2}	B	$(Webers/m^2)$	$Webers$
2-forms	m^{-2}	J	$(Amps/m^2)$	$Amps$
2-forms	m^{-2}	$E \times H$	$(Watts/m^2)$	$Watts$
3-forms	m^{-3}	$E \cdot D$	$(Joules/m^3)$	$Joules$
3-forms	m^{-3}	ρ	$(Coulombs/m^3)$	$Coulombs$

is that ours satisfy the properties in Table 1. The uniformly spaced interpolatory bases are suitable for low order approximations, *i.e.*, k = 1 to 4. It is well known that this particular choice of interpolation points produce badly conditioned mass and stiffness matrices when high order approximations are used. For this reason we have implemented spectral classes that use arbitrary sets of interpolation points, typically Gauss-Lobatto or Tchebyschev points. A study of the conditioning of finite element matrices using various higher-order $H(curl)$ discretizations is given in [33]. An additional class of semi-orthogonal basis functions was developed by the authors in order to increase the efficiency of the method. These basis functions are paired with a custom quadrature rule to minimize the number of non-zeroes in the mass matrices. This is an extension of the standard mass-lumping procedure widely used in computational mechanics. For the special case of an orthogonal Cartesian mesh the mass matrix is made diagonal, resulting in a tremendous increase in efficiency, particularly for higher-order bases applied to time dependent problems. For unstructured meshes the basis functions are not completely orthogonal but the number of non-zeros is decreased by a factor of 5 or more. While these inexact quadratures are often considered a "variational crime", in practice there is no loss of accuracy in the computed solution [34].

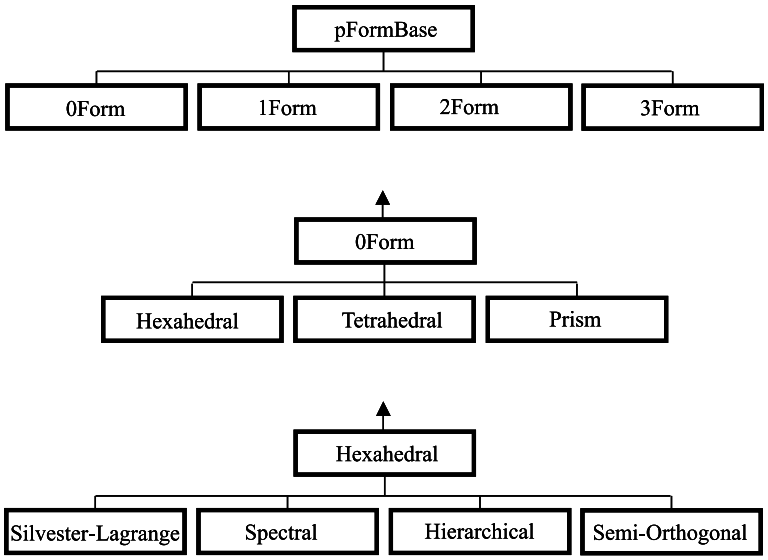

FIG. 1. *p-Form basis function class hierarchy. Only part of the hierarchy is shown. The general idea is that the Application Program Interface is defined at the higher levels, and the unique details of each type of basis function are implemented at the lower levels. Users can easily add new basis functions to the class hierarchy, and the client program need not be modified at all.*

2.2. Global Finite Element Operations. The *EMSolve* framework computes sparse matrices which are global versions of the previously described bilinear forms. The basic matrices are

$$\mathbf{M}^p(\alpha)_{ij} = \int_\Omega \alpha W_i^p \, W_j^p \, d\Omega \tag{2.14}$$

$$\mathbf{S}^p(\alpha)_{ij} = \int_\Omega \alpha dW_i^p \cdot dW_j^p \, d\Omega \tag{2.15}$$

$$\mathbf{D}^{p(p+1)}(\alpha)_{ij} = \int_\Omega \alpha dW_i^p \cdot W_j^{p+1} \, d\Omega \tag{2.16}$$

which we refer to as the "mass", "stiffness", and "derivative" matrices, respectively. The "mass" matrices **M** are square symmetric positive definite, and the "stiffness" matrices **S** are square symmetric positive semi-definite. These two matrices map p-forms to p-forms. The "derivative" matrices **D** are rectangular and map p-forms to $(p+1)$-forms. It can be shown that

$$\mathbf{D}^{p(p+1)} = \mathbf{M}^{p+1}\mathbf{K}^{p(p+1)} \tag{2.17}$$

$$\mathbf{S}^p = \left(\mathbf{K}^{p(p+1)}\right)^T \mathbf{M}^{(p+1)}\mathbf{K}^{p(p+1)} \tag{2.18}$$

where $\mathbf{K}^{p(p+1)}$ is a "topological derivative" matrix. This matrix is the discretization of the exterior derivative operator d from differential geometry, $dW^p = W^{(p+1)}$.

This matrix depends upon the mesh connectivity, but is independent of the nodal coordinates. It does not involve an integral over the element, and it does not involve any material properties. For the special case of first-order basis functions, the topological derivative matrix is a mesh incidence matrix consisting of 0's, $+1$'s, and -1's. While seemingly abstract, the topological derivative matrix is enormously valuable in practice. Given a p-form quantity X with basis function expansion

$$X = \sum_{i=1}^{n} x_i W_i^p, \tag{2.19}$$

and a $(p+1)$-form quantity Y with basis function expansion

$$Y = \sum_{i=1}^{n} y_i W_i^{(p+1)}, \tag{2.20}$$

the exterior derivative (gradient, curl, divergence for $p = 0$, $p = 1$, and $p = 2$, respectively) is given by

$$\mathbf{y} = \mathbf{K}^{p(p+1)}\mathbf{x}. \tag{2.21}$$

It can be shown that

$$\mathbf{K}^{12}\mathbf{K}^{01} = 0 \tag{2.22}$$

$$\mathbf{K}^{23}\mathbf{K}^{12} = 0 \tag{2.23}$$

which are the discrete versions of the identities $\nabla \times \nabla F = 0$ and $\nabla \cdot \nabla \times F = 0$, respectively. These identities are satisfied in the discrete sense, to machine precision, for any mesh and any order basis function. This is a key feature (perhaps the definition of) a compatible discretization. It is these identities that ensure computed solutions of Maxwell's equations are solenoidal, whether in eigenmode computations or time-dependent computations.

EMSolve contains some additional miscellaneous functionality. In some circumstances it is necessary to convert a p-form to a $(3-p)-$form, i.e. a Hodge-star operation. A classic example is converting a "cell-center" quantity to a "nodal" quantity. In our finite element setting the Galerkin procedure prescribes rectangular matrices of the form

$$\mathbf{H}_{ij}^{p(3-p)} = \int_{\Omega} W_i^p \wedge W_j^{(3-p)} \, d\Omega \tag{2.24}$$

which produces optimal (in the least-square error sense) Hodge-star operators for arbitrary order basis functions.

To summarize the overall numerical procedure employed in *EMSolve* , the first step is to identify the correct p-form for the physical quantities. This then dictates the particular basis function expansion of the physical quantity. A generic

field variable X is then approximated over each element $\Sigma \in \Sigma_h$ by a basis function expansion of the form

$$X^p(r,t) = \sum_i \alpha_i(t)\, w_i^p(r), \quad w_i^p \in W_h^p \tag{2.25}$$

where $\alpha_i(t)$ are the time-dependent p-form degrees of freedom, $w_i^p(r)$ are the spatially dependent p-form basis functions. The semi-discrete system is formed by applying the Galerkin procedure resulting in combinations of the mass matrices **M**, the stiffness matrices **S**, the derivative and topological derivative matrices **D** and **K**. The result is a systematic procedure for discretizing a wide variety of electromagnetics equations.

3. Frequency Domain Resonant Cavity Examples. The *EMSolve* framework is well suited for simulations in the frequency domain. Here we focus on the resonant cavity problem, where the goal is to compute the electromagnetic fields within closed perfectly conducting cavities that may contain dielectric and/or magnetic materials. The starting point is the vector Helmholtz equation for the electric field

$$d \star_{\mu^{-1}} dE = -\omega^2 \star_\varepsilon E \tag{3.1}$$

The electric field is chosen instead of the magnetic field because the perfect electrical conductor conductor boundary condition $n \times E = 0$ is trivial to implement when using a 1-form basis function expansion for E.

Using the Galerkin procedure described in Section 2, the linear system of equations for the discretized eigenvalue problem is

$$\mathbf{S}^{11}_{\mu^{-1}}\mathbf{e} = -\omega^2 \mathbf{M}^{11}_{\varepsilon}\mathbf{e}, \tag{3.2}$$

where **e** is the vector of 1-form degrees-of-freedom. The exact solution of (3.1) has irrotational eigenmodes corresponding to $\omega = 0$ and solenoidal eigenmodes corresponding to $\omega \neq 0$, with all these modes being orthogonal. This 1-form based discretization preserves the Helmholtz decomposition exactly, with no additional constraints. The irrotational solutions of (3.2) satisfy

$$\mathbf{e}_{irrotational} = \mathbf{K}^{01}\mathbf{f}, \tag{3.3}$$

where **f** is an arbitrary discrete scalar potential, and the solenoidal solutions of (3.2) satisfy

$$\left(\mathbf{e}_{solenoidal}\right)^T \mathbf{M}^{11}\mathbf{K}^{01}\mathbf{f} = 0, \tag{3.4}$$

i.e. they are orthogonal to the gradients of the scalar potentials. Alternative finite element discretizations using vector nodal basis functions discretizations introduced spurious modes, i.e. modes that are not solenoidal. This was first analyzed by Bossavit [35] and Cendes [36], and was historically the primary impetus for using edge-based $H(curl)$ -conforming basis functions in electromagnetics.

Applying general purpose iterative eigenvalue solvers to the $H(curl)$ discretized Helmholtz equation is often problematic due to the large null space of the system. The large degeneracy of zero-eigenvalues can cause iterative methods to fail to converge on the desired smallest non-zero eigenvalues. The authors have developed a method to shift the zero eigenvalues corresponding to the irrotational solutions of the Helmholtz equation arbitrarily to the middle of the spectrum [37]. The implicitly restarted Arnoldi method package (ARPACK) [38] is then used to solve for the smallest extremal eigenvalues which are now non-zero.

3.1. Lowest Resonant Mode for the Trispal Induction Cell. The parallel version of the ARPACK code, PARPACK, was used to determine the lowest eigenvalue and eigenmode for the Trispal induction cell. This induction cell is a key component of a proposed proton linear accelerator [39] and is used as a metric for various Helmholtz equation solvers. The Trispal geometry was decomposed into a refined and optimized tetrahedral mesh and a hexahedral mesh as shown in Figure 2. The tetrahedral mesh contained 61,566 zones and 76,838 edges while the hexahedral mesh contained 26,568 zones and 84,807 edges. Results for the

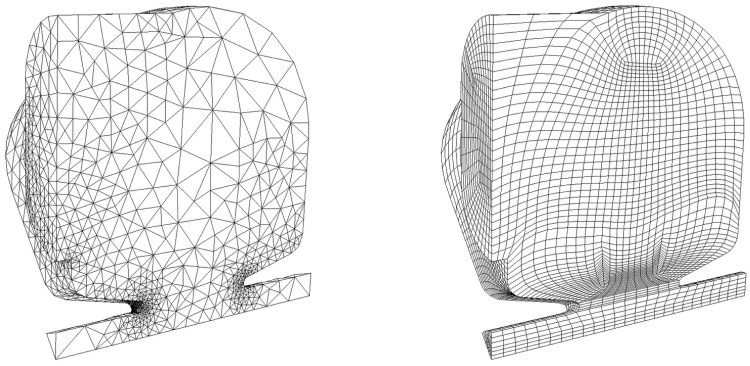

FIG. 2. *The optimized tetrahedral mesh and unoptimized hexahedral mesh for the Trispal geometry. The mesh is of 1/8 of the geometry.*

computed lowest eigenvalue with $k = 1$ basis functions compared with the measured eigenvalue, frequency=1064.415 MHz, for each mesh are shown in Table 3. The results were not any better for a higher-order $k = 2$ discretization, indicating that the accuracy for this problem is limited by the discretization of the geometry. The goal for this type of resonant cavity problem is agreement to measurement to within 0.01%, achieving this level of validation requires precise agreement of the CAD geometry and the test article. The z-component of the resulting eigenmode for the hexahedral mesh is shown in Figure 3.

4. Electromagnetic Wave Equations. Consider Maxwell's equations in a charge free region, written in the language of differential forms

$$\star_\varepsilon \frac{\partial}{\partial t} E = d(\star_{\mu^{-1}} B) - \star_\sigma E - J \tag{4.1}$$

TABLE 3
Trispal Eigenvalues

Mesh	Calculated Frequency (MHz)	Relative Error (%)
Tetrahedral	1066.45	0.19
Hexahedral	1084.12	1.85

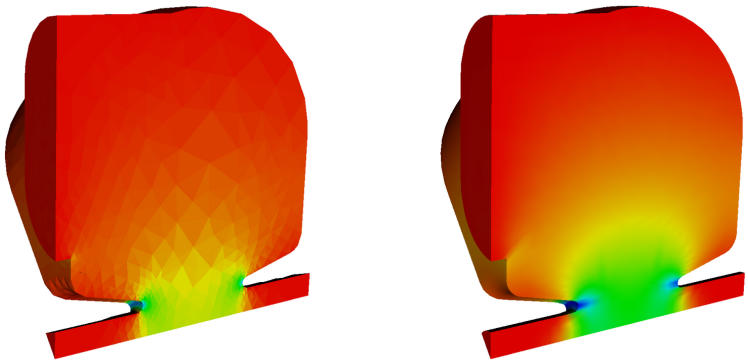

FIG. 3. *The computed Z component of the lowest electric field eigenmode for the Trispal geometry.*

$$\frac{\partial}{\partial t}B = -dE \tag{4.2}$$

$$d \star_\varepsilon E = 0 \tag{4.3}$$

$$dB = 0 \tag{4.4}$$

where the electric field E is a 1-form, the magnetic flux density B is a 2-form, J is an independent 2-form current source, and each of the material property functions are represented by a specific Hodge function. For simplicity the required boundary conditions and initial conditions are not shown here. By applying the exterior derivative operator to both (4.1) and (4.2), it is clear that the divergence constraints of (4.3) and (4.4) are constraints on the initial conditions of the fields. While this is not universally accepted, it is our opinion that a compatible discretization of Maxwell's equations will not require any penalty method or Lagrange multiplier method to satisfy the divergence constraints, they will be intrinsically satisfied by the discretization of equations (4.1) and (4.2). Of course the divergence constraints of (4.3) and (4.4) are satisfied according to a particular, but consistent, discrete metric. For the electric field the divergence is measured in the variational sense

$$\int_\Omega d \star_\varepsilon E \wedge \Phi = \int_\Omega \star_\varepsilon E \wedge d\Phi, \tag{4.5}$$

for all test functions Φ not on the boundary, since this measure allows for the jump discontinuity in E. For the magnetic flux density the divergence is computed directly.

Using the procedures described in Section 2, the semi-discrete Ampere-Faraday system of equations is

$$\begin{aligned} \mathbf{M}_{\varepsilon}^{11}\,\frac{\partial}{\partial t}\mathbf{e}(t) &= \left(\mathbf{K}^{12}\right)^{T}\mathbf{M}_{\mu}^{22}\,\mathbf{b}(t) - \mathbf{M}_{\sigma}^{11}\,\mathbf{e}(t) - \mathbf{M}_{\varepsilon}^{11}\,\mathbf{j}(t) \\ \frac{\partial}{\partial t}\mathbf{b}(t) &= -\mathbf{K}^{12}\,\mathbf{e}(t) \end{aligned} \tag{4.6}$$

where $\mathbf{e}(t)$ and $\mathbf{b}(t)$ are the vectors of unknown degrees-of-freedom. The divergence equations are discretized as

$$\begin{aligned} \left(\mathbf{K}^{01}\right)^{T}\mathbf{M}_{\varepsilon}^{11}e &= 0 \\ \mathbf{K}^{12}b &= 0 \end{aligned}$$

and by the compatibility properties (2.22)-(2.23) these conditions will be satisfied automatically, to the tolerance used in the solution of the mass matrices.

There are several methods for integrating (4.6) in time, the staggered 2nd-order central difference or "leapfrog" method being quite popular. The leapfrog method is conditionally stable and energy conserving. The leapfrog method is an example of a class of methods known as symplectic methods, which were originally developed for Hamiltonian systems. A high order and energy conserving time-integration of (4.6) is given by a generalized symplectic update [40]

$$\begin{bmatrix} \mathbf{e}_{n+1} \\ \mathbf{b}_{n+1} \end{bmatrix} = \left(\prod_{i=1}^{m} Q_i\right)\begin{bmatrix} \mathbf{e}_{n} \\ \mathbf{b}_{n} \end{bmatrix} \tag{4.7}$$

where m is the order of the symplectic integration method and the matrices Q_i are of the form

$$Q_i = \begin{bmatrix} I & \beta_i\,\Delta t\,(\mathbf{M}_{\varepsilon}^{11})^{-1}(\mathbf{K}^{12})^{T}\mathbf{M}_{\mu}^{22} \\ -\alpha_i\,\Delta t\mathbf{K}^{12} & I - \alpha_i\,\beta_i\,\Delta t^{2}\mathbf{K}^{12}\,(\mathbf{M}_{\varepsilon}^{11})^{-1}(\mathbf{K}^{12})^{T}\mathbf{M}_{\mu}^{22} \end{bmatrix} \tag{4.8}$$

and Δt is the discrete time step. The specific integration coefficients α_i and β_i of (4.8) can be found in [41]. Note that the standard definition of a symplectic integrator requires that the length of the vectors $\mathbf{e}_n$ and $\mathbf{b}_n$ be the same, and they are not in our case, hence we use the term symplectic loosely. A straightforward but tedious calculation shows that for suitably small Δt the eigenvalues of the Q_i lie on the unit circle, and the eigenvectors of Q_i are linearly independent, hence the time integration method is neutrally stable. The stability condition is given by

$$\Delta t \leq \frac{2}{\sqrt{\rho\left(\alpha_i\,\beta_i\,\mathbf{K}^{12}\,(\mathbf{M}_{\varepsilon}^{11})^{-1}(\mathbf{K}^{12})^{T}\mathbf{M}_{\mu}^{22}\right)}};\quad i=1,\ldots,m \tag{4.9}$$

where ρ denotes the spectral radius of the matrix, and in practice this is estimated by performing a few power-method iterations to estimate the largest eigenvalue. Stated another way, (4.9) requires that the sampling frequency (determined by Δt) must be less than half the highest resonant frequency of the spatial discretization. The stability condition of (4.9) is valid for all values of k, the order of the polynomial basis functions. However, as k is increased, the value of $\rho\left(\mathbf{K}^{12}\,(\mathbf{M}_{\varepsilon}^{11})^{-1}(\mathbf{K}^{12})^{T}\mathbf{M}_{\mu}^{22}\right)$ (and hence the highest resonant frequency of the spatial discretization) will grow, thus requiring a smaller time step Δt. For the special case of lossless materials and no energy entering/exiting the volume through the bounding surface the total electromagnetic energy should be constant. With this class of symplectic time integration the instantaneous energy stored in the electric and magnetic fields is

$$\mathbf{e}^{T}\mathbf{M}_{\varepsilon}^{11}\,\mathbf{e}+\mathbf{b}^{T}\mathbf{M}_{\mu}^{22}\,\mathbf{b}=\tilde{\mathcal{E}}+O(\Delta t^{k+1})sin(\omega t), \tag{4.10}$$

the energy oscillates about the constant value $\tilde{\mathcal{E}}$. This is in contrast to non-symplectic methods such as Runge-Kutta, in which the energy is a monotonically decaying function. In [42] it is shown that the symplectic update method can be extended to include electric and magnetic conductivity, for example artificial Perfectly Matched Layers.

4.1. Transmission in a Bent Optical Fiber. There is great interest in analyzing the performance of bent optical fibers [43], [44]. A weak bend can be analyzed using efficient paraxial beam propagation methods, here we demonstrate an accurate full wave simulation of a fiber with an extreme bend. We visualize the propagation of an optical pulse along a $155\mu m$ section of a step index optical fiber. The core of the fiber has a radius of $5\mu m$ and an index of refraction of 1.471 while the cladding has a radius of $40\mu m$ and an index of refraction of 1.456. With these properties, the fiber is capable of propagating a $\lambda = 1.55\mu m$ optical wave. The ratio of problem domain size to wavelength is therefore $\Omega/\lambda = 100$ making this an "electrically large" problem. The problem is excited with a space and time dependent Dirichlet boundary condition applied to the input cap of the fiber representing a TE01 polarized pulse.

We perform the simulation using a straight fiber as reference and four bent fibers with different bend angles. Because the problem is electrically large, it will be subject to the cumulative errors of numerical dispersion. To mitigate this effect, we use high order polynomial basis functions of degree $k = 2$ in conjunction with a high order symplectic (energy conserving) integrator of order $m = 3$ which has been shown to excel at reducing the effects of numerical dispersion for electrically large time domain problems [40]. The computational mesh for each of the five simulations consists of $147,200$ hexahedral elements with 4 transverse elements per wavelength, an example of which is shown in Figure 4. Using high order $k = 2$ basis functions on this mesh results in a semi-discrete linear system (4.6) consisting of $3,562,160$ electric field unknowns and $3,547,072$ magnetic flux density unknowns. This relatively large problem must therefore be solved in a parallel computational environment. In Figure 5 we plot the normalized energy in

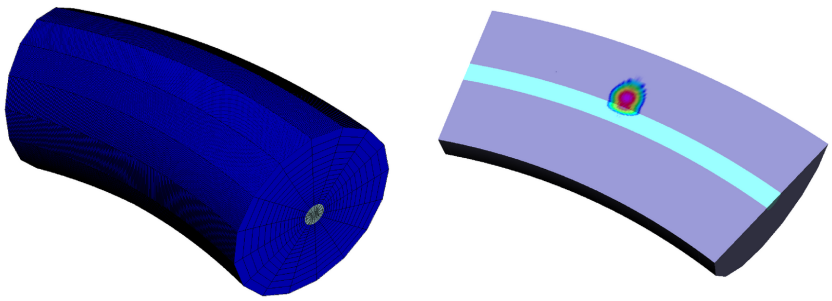

FIG. 4. *Example of bent optical fiber mesh (*left*) and snapshot of the electromagnetic energy in the 30 degree bent fiber at time* $t = 0.4ps$.

the fiber core, computed by (4.10), as a function of time for each of the five fiber simulations. The energy is normalized to the total energy of the optical pulse. As expected, the total pulse energy is conserved. As the fiber is bent, the energy in the core is lost due to radiation in the cladding as the pulse traverses the bend. This effect becomes more drastic as the bend angle increases and as time increases.

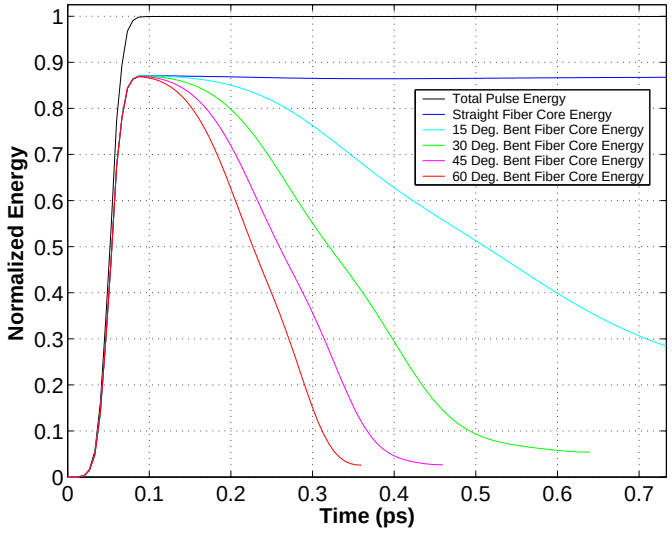

FIG. 5. *Normalized core energy as a function of time for five fiber simulations.*

4.2. 3D Photonic Crystal Waveguide. Here we simulate a 3D PBG waveguide with a complete photonic band-gap designed to operate in the RF regime. The PBG crystal is based on the "woodpile" structure as investigated by [45]. In

particular, we utilize the unit cell originally proposed by [46] which consists of a series of aluminum rods (index of refraction $= 3.1$) arranged in an alternating, stacked configuration. The lattice constant for this crystal is $1.123cm$ and the unit cell has dimensions of $1.123cm$ by $1.123cm$ by $1.272cm$ making it suitable for operation in the radio frequency regime. We construct a 3D crystal by arranging the unit cell in a 9 by 13 by 7 layer configuration as shown in Figure 6. Our goal is to exploit the complete photonic band gap of this crystal and create a "multi-bend" wave guide where we can make the radio signal traverse two separate 90 degree bends in three dimensional space. Because of the 3D nature of the multi-bend, this type of simulation cannot be performed using standard 2D codes which are extensively used in the study of PBG devices. In addition, trustworthy simulations of PBG waveguides require that phase velocities of propagating waves be computed as accurately as possible. A high order method is therefore highly desirable for an electrically large waveguide such as this.

The computational mesh of Figure 6 consists of $419,328$ hexahedral elements. We excite the problem with a time dependent Dirichlet boundary condition applied at the *x*-*z* input plane with an operating frequency of $11GHz$. The rest of the mesh is terminated with a PEC boundary condition. We use high order $k = 2$ basis functions to represent the electric and magnetic fields resulting in a linear system with approximately 10.5 million unknowns. This large linear systems requires that the problem be distributed in parallel across 150 processors. We let the simulation run for a total of $6,500$ time steps. In Figure 7 we show a three dimensional iso-surface plot of the electric field magnitude in the wave guide at the end of the simulation. Note how the wave has made two complete 90 degree bends with a negligible loss due to radiation.

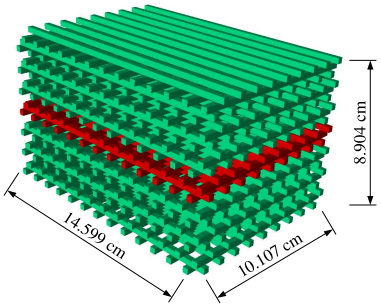

FIG. 6. *3D PBG "woodpile" structure for RF signals. The portion of the mesh representing the air has been removed for visual clarity.*

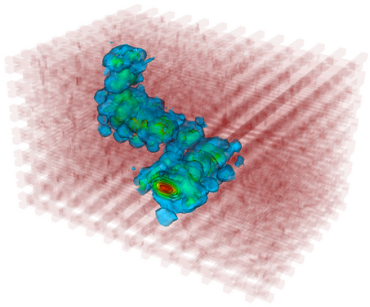

FIG. 7. *Three dimensional iso-surface plot of electric field magnitude for the 3D PBG simulation.*

4.3. Simulation of Magnetic Resonance Imaging. When a magnetic field penetrates a conducting object, eddy currents are produced. These eddy currents modify the magnetic field resulting in a non-uniform magnetic field in the conductor. This fact is of significant relevance in the field of magnetic resonance

imaging (MRI) where the characterization of field non-uniformities inside of a human head are of great research interest. In a typical MRI experiment, a very large (1-8 Tesla) and static magnetic field (called the $B0$ field) is used to align the magnetic moments of atomic nuclei inside of a human tissue sample. A secondary pulsed RF field (called the $B1$ field) is used to tip the magnetic moments when turned on. When turned off, the magnetic moments relax back to their original state, emitting radiation that is detected by an RF receiver. The $B1$ field determines image intensity and imaging algorithms assume a spatially uniform $B1$ field; non-uniform $B1$ fields lead to artificial variation in image intensity. If the actual non-uniform magnetic field were known, it might be possible to correct for this in the image processing.

Unlike the previous examples which involved propagation in a loss-less region, this application requires the introduction of a lossy term due to finite electrical conductivity. Also, the goal here is to reach a sinusoidal steady-state solution, and due to the fine mesh a very large number of time steps would be required if conditionally stable time integration method were used. We therefore employ an implicit time integration method. In particular, we use the implicit Newmark-Beta method given by

$$\begin{aligned}(4.11)\quad &\left(\mathbf{M}_{\varepsilon}^{11}+\beta\Delta t^2\mathbf{S}_{\mu^{-1}}^{11}+\frac{dt}{2}\mathbf{M}_{\sigma}^{11}\right)\mathbf{e}_{n+1}=\left(2\mathbf{M}_{\varepsilon}^{11}-(1-2\beta)\Delta t^2\mathbf{S}_{\mu^{-1}}^{11}\right)\mathbf{e}_n\\ &-\left(\mathbf{M}_{\varepsilon}^{11}+\beta\Delta t^2\mathbf{S}_{\mu^{-1}}^{11}-\frac{dt}{2}\mathbf{M}_{\sigma}^{11}\right)\mathbf{e}_{n-1}-dt^2\mathbf{M}^{11}\mathbf{j}_n'\end{aligned}$$

Note that this is a fully discrete version of the second order electric field wave equation (2.10) with the addition of a lossy conductive term.

In this example we use *EMSolve* to compute the eddy currents and non-uniform magnetic field inside a $10cm$ conducting, dielectric sphere immersed in a spatially uniform and time varying 200 MHz $B1$ magnetic field. The external $B1$ field is created by a pair of Helmholtz coils, driven by a 200 MHz sinusoidal current source represented by the $\mathbf{j}_n'$ term in (4.11). A human head is modeled by a conducting dielectric sphere of conductivity $\sigma = 0.5S/m$ and dielectric constant $85\varepsilon_0$ as shown in Figure 8. The fully discrete (4.11) is solved for a net physical time equal to 10 periods of $B1$ field oscillation, enough time for the induced eddy currents to reach a steady state. In Figure 9 we show the induced eddy currents and the resulting non-uniform magnetic field inside of the sphere. Note the appearance of the so called "central-brightening" effect in the magnetic field magnitude, a result in agreement with the theoretical calculations of [47], [48]. Results such as these can be used to calibrate MRI images to account for the non-uniformity of the $B1$ field.

5. Electromagnetic Diffusion Equations. Solution of the Ampere-Faraday system of equations (4.1)-(4.2) are electromagnetic waves that propagate at the speed of light in the medium. However in many applications the time scales are such that it is not desired to resolve the wave nature of the fields. In some

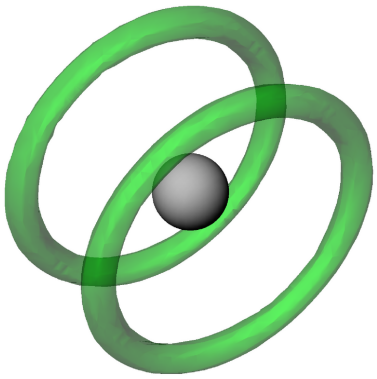

FIG. 8. *Conducting dielectric sphere representing a human head placed between two Helmholtz coils.*

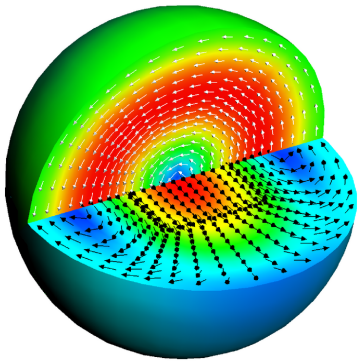

FIG. 9. *Computed eddy currents (*vertical plane*) and non-uniform magnetic field (*horizontal plane*) inside of conducting dielectric sphere.*

problems the electric field satisfies

$$\left| \star_\varepsilon \frac{\partial}{\partial t} E \right| \ll |\star_\sigma E| \tag{5.1}$$

and the $\star_\varepsilon \frac{\partial}{\partial t} E$ term can be neglected without serious consequence. This is a definition of a good conductor, for example copper with $\varepsilon = 8.854 \cdot 10^{-12}$ and $\sigma = 5.76 \cdot 10^7$ is a good conductor for frequencies up to the MHz range. The electric field is not zero in a good conductor, rather the correct statement is that in a good conductor the displacement current is negligible compared to the conduction current. To continue with the copper example, a dimensional analysis indicates a characteristic field diffusion time of $\tau = \sigma \mu L^2$ where L is the characteristic dimension of the block. Using $\mu = 4\pi \cdot 10^{-7}$ and $L = 1m$, this diffusion time is several orders of magnitude longer than the time it takes the EM wave to traverse the conductor. By not resolving the EM wave, we do not have stability conditions or accuracy conditions that involve the speed of light. This is the motivation for ignoring the displacement current term.

Neglecting the displacement current, Maxwell's equations become

$$d(\star_{\mu^{-1}} B) - \star_\sigma E - J = 0 \tag{5.2}$$

$$\frac{\partial}{\partial t} B = -dE \tag{5.3}$$

$$d \star_\sigma E = 0 \tag{5.4}$$

$$dB = 0 \tag{5.5}$$

Note that (5.4) is not independent from (5.2), it is a consequence of the identity $dd\psi = 0$ (we assume the independent source satisfies $dJ = 0$ also.) Likewise,

(5.5) is not completely independent of (5.3), as clearly we will have $dB = 0$ for all time if it is satisfied initially. While not necessary, we will employ potentials to solve this problem. Equation (5.5) implies that $B = dA$ for some magnetic vector potential A. Replacing B with dA in (5.3) gives $E = -\frac{\partial}{\partial t}A - d\phi$ where ϕ is some scalar electric potential. At present ϕ is somewhat arbitrary, and ϕ can be made to agree with the standard electrostatic potential by enforcing the Coulomb gauge condition on A, resulting in

$$d \star_\sigma A = 0 \tag{5.6}$$

$$d \star_\sigma d\phi = 0 \tag{5.7}$$

Combining these equations gives a diffusion equation for A,

$$\star_\sigma \frac{\partial A}{\partial t} = d \star_{\mu^{-1}} dA - \star_\sigma d\phi - J, \tag{5.8}$$

which along with the the constraints (5.6) and (5.7) and appropriate boundary conditions provides a well-posed PDE. Note that as in the discretization of the full-wave Maxwell's equations in Section 4, the divergence constraint on the 1-form field, in this case (5.6), will be implicitly satisfied for all time if it is initially satisfied. The advantage of this formulation compared to an H-based method or an E-based method is that the electrostatic potential ϕ appears explicitly in the PDE, this is useful in solving engineering problems in which the voltage across a conductor is the known boundary condition. The disadvantage of the A-ϕ approach is of course the required elliptic solve for (5.7), but with the advent of scalable multi-grid solvers this is less of an issue than it used to be.

Again using the definitions in Section 2, the semi-discrete equations are given by

$$\mathbf{M}_\sigma^{11} \frac{\partial}{\partial t}\mathbf{a} = -\mathbf{S}_\mu^{11}\mathbf{a} - \mathbf{D}_\sigma^{01}\mathbf{v} + \mathbf{j}^1 \tag{5.9}$$

$$\mathbf{S}_\sigma^{00}\mathbf{v} = \mathbf{f}^0 \tag{5.10}$$

where $\mathbf{a}$ is the vector of degrees-of-freedom of A, $\mathbf{v}$ is the vector of degrees-of-freedom of ϕ, and $\mathbf{j}$ and $\mathbf{f}$ are the discrete volume and surface source terms, respectively.

Given A, it is possible to compute the magnetic flux density B, the electric field E, and the electric current density J. Since A is a 1-form and B is a 2-form and $B = \nabla \times A$ we have

$$\mathbf{b} = \mathbf{K}^{12}\mathbf{a}. \tag{5.11}$$

This is a purely topological operation, no integration or material properties are involved. The computation of E is also trivial, using $\mathbf{e}$ to denote the degrees-of-freedom for the electric field, the semi-discrete electric field equation is

$$\mathbf{e} = -\frac{\partial}{\partial t}\mathbf{a} - \mathbf{K}^{01}\mathbf{v}. \tag{5.12}$$

If required, a 2-form electric current J can be computed from $J = \sigma E$, this is an example of a Hodge-star operation and requires the inversion of a "mass" matrix.

For the numerical time integration, we apply a generalized Crank-Nicholson method by averaging a first-order forward difference at time n with a first-order backward difference at time $(n+1)$. The averaging is performed with a weighting parameter α, where $0 \leq \alpha \leq 1$, such that

$$\alpha = \begin{cases} 0 & \text{Explicit, 1st Order Accurate Forward Euler} \\ 1/2 & \text{Implicit, 2nd Order Accurate Crank Nicholson} \\ 1 & \text{Implicit, 1st Order Accurate Backward Euler} \end{cases}$$

The fully discrete equations are given by

$$\mathbf{S}^{00}\mathbf{v}_{n+\alpha} = \mathbf{f}^0 \tag{5.13}$$

$$\begin{aligned} \left(\mathbf{M}^{11}_{\sigma} + \alpha\Delta t \mathbf{S}^{11}_{\mu^{-1}}\right)\mathbf{a}_{n+1} = &\left(\mathbf{M}^{11}_{\sigma} - (1-\alpha)\Delta t \mathbf{S}^{11}_{\mu^{-1}}\right)\mathbf{a}_n \\ &-\Delta t \mathbf{D}^{01}\mathbf{v}_{n+\alpha} + \Delta t \mathbf{j}^1 \end{aligned} \tag{5.14}$$

$$\mathbf{b}_{n+1} = \mathbf{K}^{12}\mathbf{a}_{n+1} \tag{5.15}$$

$$\mathbf{e}_{n+\alpha} = -1/\Delta t\,(\mathbf{a}_{n+1} - \mathbf{a}_n) - \mathbf{K}^{01}\mathbf{v}_{n+\alpha} \tag{5.16}$$

$$\mathbf{M}^{22}_{\sigma^{-1}}\mathbf{j}_{n+\alpha} = \mathbf{H}^{12}\mathbf{e}_{n+\alpha} \tag{5.17}$$

where it is assumed that the boundary conditions and current sources can be evaluated at $t = n+\alpha$. Note that to maintain second order accuracy for all variables, the magnetic potential A and the magnetic flux B are known at whole times n, whereas the electric potential Φ and the electric field E are known at intermediate times $(n+\alpha)$. For some problems, striving for accuracy by using $\alpha = 1/2$ will lead to oscillations in the computed solution, and in such cases it is necessary to use standard Backward Euler ($\alpha = 1$).

5.1. Electromagnetic Heating and Forces in a Simple Rail Gun Model. In this example we use the vector potential formulation of the electromagnetic diffusion equations to compute the $J \times B$ forces and $J \cdot E$ joule heating in a simple rail-gun model. A rail-gun is a device used to launch projectiles using only electromagnetic energy and accurate characterization of the electromagnetic forces and heating is required for trustworthy modeling. The rail gun model consists of two conducting rails and a sliding armature placed between them. Note that in this simple simulation, the motion of the armature is not taken into account, we are simply computing the transient eddy currents and magnetic fields for the case of a fixed armature. The motion of the armature will effect the fields when the velocity is comparable to the diffusion time. The rails and armature are placed in a cubic mesh representing the air. In reality, the conductivity of the air is essentially zero, however due to the nature of the FEM discretization, we cannot simply set this term to zero in the air region, so we make it significantly smaller (7 orders of magnitude) than the conductivity of the rails and armature. While not an elegant solution, this great disparity in conductivity is a good test of the proposed formulation. The problem is driven by applying a constant voltage difference across the

rail inputs. At time $t = 0$, the scalar Poisson equation is solved via a fast multi-grid method to compute the static scalar potential everywhere in space. This in turn induces transient eddy currents and magnetic fields which gradually build over time to steady state value as shown in Figure 10. The fully discrete vector potential equation (5.15) using $\alpha = 1/2$ is solved at every time step using a diagonally scaled Pre-conditioned Conjugate Gradient (PCG) method with a relative residual error tolerance of 10^{-10}. This linear solver required an average of 300 PCG iterations, in spite of the large contrast in conductivity values. PCG worked well for this relatively modest problem with $161,280$ elements and $\sim 500,000$ unknowns, but for larger problems PCG is impractical; a scalable multigrid solver tuned for the $\nabla \times \nabla \times$ operator should be used [49] [50]. In Figure 11 we plot the computed vector force field and scalar Joule heat field for two different armature positions. Note that a net outward force is generated and the Joule heating is strongest at the corners of the armature contact position. Note also that as the armature is moved further along the rails, the net inductance and resistance of the rail gun circuit increases, causing the induced force and heat to decrease.

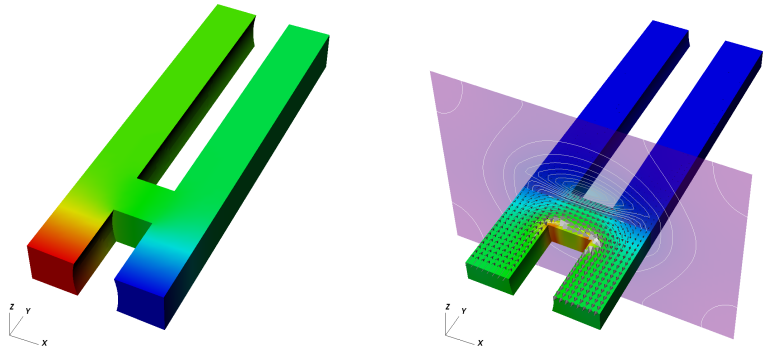

FIG. 10. *Computed scalar potential (*left*) and steady state eddy currents and magnetic fields (*right*) in a simple rail gun model.*

6. Conclusions. When the Galerkin finite element method is applied to electromagnetics problems using the standard nodal shape functions the results are quite disappointing, and fail to converge for even trivial problems. While adding penalty terms or Lagrange multipliers involving the divergence of the fields improves the situation, these methods cannot be considered a fundamental cure. The problem is not with the Galerkin procedure *per se*, but with the choice of finite element basis functions. Numerous researchers have proposed various $H(curl)$ -conforming and $H(div)$ -conforming based finite element basis functions that result in provably stable discrete variational formulations of electromagnetics problems. Aspects of differential forms such as exact sequences have had a significant impact on the development of these basis functions. In addition, we believe that differential forms provide a unified way for organizing and implementing a

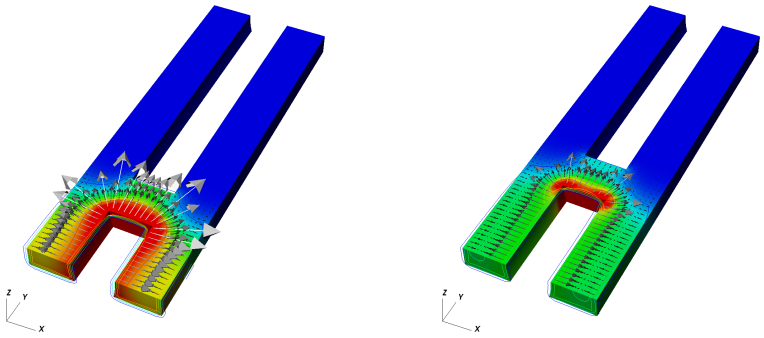

FIG. 11. *Computed $J \times B$ force field and $J \cdot E$ joule heating for two different armature positions.*

sophisticated simulation code so that it can be used to solve a wide class of problems, in fact virtually any problem that can be expressed in the language of differential forms. This has been demonstrated in the context of electromagnetics with the *EMSolve* code. However not all PDE's can be simply cast in the language of differential forms. Developing compatible discretizations for multi-physics problems, that involve not just curl and divergence equations but also advection of materials and fields, is likely to be an important area of future research.

REFERENCES

[1] G. Deschamps. Electromagnetics and differential forms. *IEEE Proceedings.*, 69(6):676–687, 1981.

[2] D. Baldomir. Differential forms and electromagnetism in 3-dimensional Euclidean space R3. *IEEE Proceedings.*, 133(3):139–143, 1986.

[3] A. Bossavit. *Computational Electromagnetism: Variational Formulation, Complementarity, Edge Elements.* Academic Press, 1998.

[4] R. Abraham, J. E. Marsden, and T. Ratiu. *Manifolds, Tensor Analysis, and Applications*. Applied Mathematical Sciences. Springer Verlag, second edition edition, 1996.

[5] H. Whitney. *Geometric Integration Theory*. Princeton University Press, 1957.

[6] J. C. Nédélec. Mixed finite elements in R3. *Numer. Math.*, 35:315–341, 1980.

[7] J. C. Nédélec. A new family of mixed finite elements in R3. *Numer. Math.*, 50:57–81, 1986.

[8] P.A. Raviart and J.M. Thomas. A Mixed Finite Element Method for 2^{nd} Order Elliptic Problems. In I. Galligani and E. Mayera, editors, *Mathematical Aspects of the Finite Element Method*, volume 606 of *Lect. Notes. on Mathematics*, pages 293–315. Springer Verlag, 1977.

[9] F. Brezzi and M. Fortin. *Mixed and Hybrid Finite Element Methods*. Springer Series in Computational Mathematics. Springer Verlag, 1991.

[10] R. Hiptmair. Canonical construction of finite elements. *Math. Comp.*, 68(228):1325–1346, 1999.

[11] I. Babuska, T. Strouboulis, C.S. Upadhyay, and S. K. Gangaraj. A posteriori estimation and adaptive control of the pollution error in the *h*-version of the finite element method for finite element solution of Helmholtz. *Internat. J. Numer. Methods Engrg.*, 38(24):4207–4235, 1995.

[12] I. Babuska, F. Ihlenburg, T. Strouboulis, and S. K. Gangaraj. A posteriori error estimation for

finite element solution of Helmholtz. *Internat. J. Numer. Methods Engrg.*, 40(21):3883–3900, 1997.

[13] S. Warren and W. Scott. An investigation of numerical dispersion in the vector finite element method using quadrilateral elements. *IEEE Trans. Ant. Prop.*, 42(11):1502–1508, 1994.

[14] S. Warren and W. Scott. Numerical dispersion in the finite element method using triangular edge elements. *Opt. Tech. Lett.*, 9(6):315–319, 1995.

[15] D. A. White. Numerical dispersion of a vector finite element method on skewed hexahedral grids. *Commun. Numer. Meth. Engng.*, 16:47–55, 2000.

[16] M. Ainsworth. Dispersive properties of high-order Nedelec/edge element approximation of the time-harmonic Maxwell equations. *Philisophical Transactions of the Royal Society of London*, 362(1816):471–491, 2004.

[17] E. Tonti. A direct formulation of field laws: The cell method. *CMES*, 2(2):237–258, 2001.

[18] T. Weiland. Time domain electromagnetic field computation with finite difference methods. *Int. J. Numer. Modelling*, 9:295–319, 1996.

[19] M. Clemens and T. Weiland. Discrete electromagnetism with the finite integration technique. In F. Texeira, editor, *Geometric Methods for Computational Electromagnetics*, volume 32 of PIER, pages 189–206. EMW Publishing, Cambridge, MA, 2001.

[20] J. M. Hyman and M. J. Shashkov. Mimetic discretizations for maxwell's equations. *J. Comput. Phys.*, 151(2):881–909, 1999.

[21] K. S. Yee. Numerical solution of initial boundary value problems involving Maxwell's equations in isotropic media. *IEEE Trans. Ant. Prop.*, 14(3):302–307, 1966.

[22] F. L. Teixeira and W. C. Chew. Lattice electromagnetic theory from a topological viewpoint. *J. Math. Phys.*, 40(1):169–187, 1999.

[23] F. L. Teixeira. *Geometric Methods in Computational Electromagnetics*, volume PIER 32. EMW Publishing, Cambridge, Mass., 2001.

[24] R. Hiptmair. Discrete Hodge operators: An algebraic perspective. *J. Electromagnteic Waves Appl.*, 15(3):343–344, 2001.

[25] D. N. Arnold and F. Brezzi. Mixed andnonconforming finite elememnt methods: implementation, postprocessing, and error estimates. *Math. Modelling and Numer. Anal.*, 19:7–32, 1985.

[26] D. N. Arnold. Mixed finite element methods for elliptic problems. *Comput. Methods Appl. Mech. Engrg.*, 82(1-3):281–300, 1990.

[27] P. G. Ciarlet. *The Finite Element Method for Elliptic Problems*. North-Holland, 1978.

[28] R. Graglia, D. Wilton, and A. Peterson. Higher order interpolatory vector bases for computational electromagnetics. *IEEE Trans. Ant. Prop.*, 45(3):329–342, 1997.

[29] R. Graglia, P. Wilton, A. Peterson, and I.-L. Gheorma. Higher order interpolatory vector bases on prism elements. *IEEE Trans. Ant. Prop.*, 46(3):442–450, 1998.

[30] P. Castillo, R. Rieben, and D. White. FEMSTER: An object oriented class library of discrete differential forms. *ACM Trans. Math. Soft.* in press.

[31] P. Castillo, R. Rieben, and D. White. FEMSTER: An object oriented class library of discrete differential forms. In *Proceedings of the 2003 IEEE International Antennas and Propagation Symposium*, volume 2, pages 181–184, Columbus, Ohio, June 2003.

[32] P. Castillo, J.Koning, R. Rieben, M. Stowell, and D. White. Discrete differential forms: A novel methodology for robust computational electromagnetics. Technical Report UCRL-ID-151522, Lawrence Livermore National Laboratory, Center for Applied Scientific Computing, January 2003.

[33] R. Rieben, D. White, and G. Rodrigue. Improved conditioning of finite element matrices using new high order interpolatory bases. *IEEE Trans. Ant. Prop.*, 52(10):2675–2683, October 2004.

[34] A. Fisher, R. Rieben, G. Rodrigue, and D. White. A generalized mass lumping technique for vector finite element solutions of the time dependent maxwell equations. *IEEE Trans. Ant. Prop.*, December 2004. accepted for publication.

[35] A. Bossavit. Solving Maxwell equations in a closed cavity, and the question of spurious modes. *IEEE Trans. Mag.*, 26(2):702–705, 1990.

[36] Z. J. Cendes. Vector finite elements for electromagnetic field computation. *IEEE Trans. Mag.*, 27(5):3958–3966, 1991.

[37] D. A. White and J. M. Koning. Computing solenoidal eigenmodes of the vector Helmholtz equation: a novel approach. *IEEE Trans. Mag.*, 38(5):3420–3425, 2002.

[38] R. Lehoucq, D. Sorenson, and C. Yang. *ARPACK User's Guide: Solution of Large Scale Eigenvalue Problems with Implicitly Restarted Arnoldi Methods*. SIAM, 1998.

[39] P. Balleyguier. Coupling slots measurements against simulation for Trispal accelerating cavities. In *Linac '98*, page 130. Chicago, 1998.

[40] R. Rieben, G. Rodrigue, and D. White. A high order mixed vector finite element method for solving the time dependent Maxwell equations on unstructured grids. *J. Comput. Phys.*, 204(2):490–519, April 2005.

[41] R. Rieben, D. White, and G. Rodrigue. High order symplectic integration methods for finite element solutions to time dependent maxwell equations. *IEEE Trans. Ant. Prop.*, 52(8):2190–2195, August 2004.

[42] R. N. Rieben. *A Novel High Order Time Domain Vector Finite Element Method for the Simulation of Electromagnetic Devices*. PhD thesis, University of California at Davis, Livermore, California, 2004.

[43] D. Marcuse. Curvature loss formula for optical fibers. *J. Opt. Soc. Am.*, 66(3):216–220, 1976.

[44] J. Koning, R. Rieben, and G. Rodrigue. Vector finite element modeling of the full-wave Maxwell equations to evaluate power loss in bent optical fibers. *IEEE/OSA J. Lightwave Tech.*, May 2005. article in press.

[45] H. S. Sözüer and J.P. Dowling. Photonic band calculations for woodpile structures. *J. Mod. Opt.*, 41(2):231–239, 1994.

[46] E Özbay, A. Abeyta, G. Tuttle, M. Trinigides, R. Biswas, C.T. Chan, C.M Soukoulis, and K.M. Ho. Measurement of a three-dimensional photonic band gap in a crystal structure made of dielectric rods. *Phys. Rev. B*, 50(3):1945–1948, 1994.

[47] D. I. Hoult. Sensitivity and power deposition in high-field imaging experiment. *J. Magn. Reson. Imag.*, 12:46–67, 200.

[48] J. S. Tropp. Image brightening in samples of high dielectric constant. *J. Magnetic Resonance*, 167(1):12–24, 2004.

[49] P. Bochev, C. Garasi, J. Hu, A. Robinson, and R. Tuminaro. An improved algebraic multigrid method for solving maxwell's equations. *SIAM J. Sci. Comp.*, 25(2):623–642, 2003.

[50] S. Reitzinger and J. Schoberl. An algebraic multigrid method for finite element discretization with edge elements. *Numer. Linear Algebra Appl.*, 9:223–238, 2002.